2015 American Control Conference
Palmer House Hilton
July 1-3, 2015. Chicago, IL, USA

Nanoscale track-following for tape storage

Angeliki Pantazi, Simeon Furrer, Hugo E. Rothuizen, Giovanni Cherubini, Jens Jelitto and Mark A. Lantz

Abstract— **Track-density scaling is projected to be the key driver for increasing the areal density and cartridge capacity in future tape storage systems. To achieve very high track densities, positioning control down to the nanometer scale will be essential. In this paper, the positioning accuracy of the tape track-following control system is investigated and advances in several elements of the system are presented. First, we introduce an optimized servo channel that combined with an experimental timing-based servo pattern provides lateral position estimates with nanoscale resolution. Second, a newly developed prototype head actuator and an experimental tape transport system were developed. The lateral tape motion (LTM) disturbance in the experimental tape path and the measurement noise in the position estimate were fully characterized and used to optimize the design of the track-following controller using the H_∞ control framework. Finally, the hardware platform used to implement the servo channel and track-following control loop was optimized to minimize loop delay. Combining these technologies with a high-SNR magnetic tape based on perpendicularly-oriented barium ferrite (BaFe) particles, we were able to demonstrate a position error signal (PES) with a standard deviation of less than 10 nm over a wide range of tape velocities.**

I. Introduction

Today's knowledge society is witnessing a continuing exponential growth in the amount of digital data that is produced and archived, driving the demand for cost-effective storage technologies. Magnetic tape systems constitute an integral part of current tiered storage infrastructures, as they are well suited for long-term storage of data thanks to their low total cost of ownership, low power consumption, very high reliability and long media lifetime. To meet the growing need for cost-effective storage, it is critical to continue to scale the areal density and the cartridge capacity of tape systems. Areal density gains have been achieved in the past by scaling both the linear recording density and the track density by similar factors. Recently, however, it has become increasingly difficult to maintain the rate of linear density scaling. The International Storage Industry Consortium (INSIC) 2012-2022 tape roadmap [1] projects the continued scaling of the areal density by about 33% a year, leading to a tape cartridge capacity of 128 TB by the year 2022. In this projection, the track-density scaling carries the biggest share with 23% a year, with a target track density of about 50000 tracks per inch by the year 2022, corresponding to a track width of 480 nm, in comparison to a linear density scaling of 8% a year. Consequently, a very high accuracy of the order of 10 nm needs to be achieved in the positioning of the read/write head with respect to tape. The viability of continuing to scale the tape areal density as indicated by the INSIC roadmap was recently demonstrated by a single-channel areal-density demonstration of 85.9 Gbit/in^2 on a new barium ferrite (BaFe) tape medium [2]. Key elements in achieving the new areal-density record are enhanced track-following servo technologies, which allow a significant improvement in the head positioning accuracy over previously reported results [3,4].

In state-of-the-art tape drives, the misalignment of the head is measured by means of position information pre-formatted in dedicated servo bands on the magnetic tape. The position error signal (PES) is used by a feedback controller that drives an actuator to adjust the position of the head to follow disturbances that are mainly due to lateral tape motion (LTM). According to the 2012 INSIC tape roadmap, existing commercial tape drives achieve a positioning accuracy characterized by a PES with a standard deviation of approximately 100 nm. Several factors impact the achievable track-following performance, including the servo reader geometry, the media signal-to-noise ratio (SNR), the servo format, the servo channel, the tape path, the actuator, and the track-following controller. In this work, we describe improvements in track-following servo technologies that lead to a head positioning accuracy of 10 nm or less over a tape speed range of 1.23 to 4.08 m/s. This range corresponds to the full speed range of an IBM[1] TS1140 enterprise class tape drive.

The paper is organized as follows. We present in Sect. II the servo pattern and the enhanced synchronous servo channel, in Sect. III the characteristics of the head actuator, in Sect. IV the tape path and LTM disturbances, in Sect. V the track-following H_∞ control system, in Sect. VI the track-following performance, and finally, in Sect. VII, we summarize the results and present our conclusions.

II. Servo pattern and Servo Channel

The servo pattern considered in this work is the experimental servo pattern described in [3], which is a variant of the timing-based servo (TBS) format that is adopted in commercial LTO tape systems [5]. The pre-

A. Pantazi, S. Furrer, H. E. Rothuizen, G. Cherubini, J. Jelitto and M. A. Lantz are with IBM Research - Zurich, 8803 Rüschlikon, Switzerland (e-mails:agp@zurich.ibm.com, sfu@zurich.ibm.com, rth@zurich.ibm.com, cbi@zurich.ibm.com, jje@zurich.ibm.com, mla@zurich.ibm.com).

[1]IBM is a trademark of International Business Machines Corporation, registered in many jurisdictions worldwide.

recorded servo pattern is characterized by azimuth angles of ±18º, a distance of 3 µm between servo stripes within a servo burst, and a frame length of 100 µm, as illustrated in Fig. 1. Relative to a conventional LTO servo format, the higher absolute value of azimuth angles reduces the position estimation noise. Recall that in TBS systems the lateral position of the head while reading the servo patterns is derived from the relative timing of bursts of dibits in the servo readback waveform, which are obtained from servo patterns with opposite or identical azimuth angles. The smaller frame length yields a twofold increase in the rate at which position estimates are generated relative to the conventional LTO servo pattern.

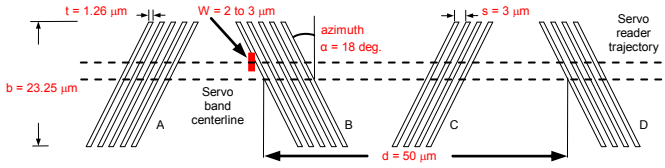

Figure 1. Layout and parameters of the experimental servo pattern [3].

In addition to estimates of lateral position, estimates of tape velocity and longitudinal position are also obtained by processing the servo readback waveform. The computation of the estimates is performed by a digital synchronous servo channel that processes the samples of the servo signals obtained by an analog-to-digital converter (ADC), which samples the servo waveform at a fixed clock rate. The signal samples are interpolated using a digital interpolator to generate a fixed number of samples per unit of tape length, independently of the tape velocity. This enables optimum detection of the servo patterns by a matched filter with a time invariant impulse response, which is provided by identification of the servo signal characteristics. Signal identification takes into account effects to be ascribed to the servo reader geometry, the servo pattern parameters, and the perpendicular BaFe media [6]. The basic functions of a synchronous servo channel were first described in [7].

Several changes were made to the servo channel implementation adopted in [3] to improve the accuracy of the lateral position. The sampling interval chosen for interpolation is a trade-off between the need to have a span of the filter impulse response that corresponds to the dispersion of a dibit, and the need to avoid aliasing effects that would arise if the sampling interval is large compared to the peak-to-peak distance that characterizes a dibit. As the dibit peak-to-peak distance is smaller for perpendicular media in comparison to non-oriented or longitudinal media [6], the interpolation sampling interval was reduced from 180 to 120 nm, and the number of coefficients in the matched filter was increased from 12 to 16. Further improvements were obtained by increasing the ADC sampling rate from 16 to 40 MHz, and the resolution of the filter coefficients from 4 to 6 bits. The combination of the improved channel with the experimental pattern on perpendicular media leads to an estimated position measurement resolution of approximately 6 nm as shown in Section IV.

III. Head Actuator

The head-actuator assembly used for this work is based on a single-stage, stripped-down version of a commercial tape drive head actuator which has been modified to increase its actuation bandwidth by lightening it and stiffening its suspension. Its principal components are shown in the schematic of Fig. 2.

The head located at the front consists of a single module of transducer elements (whereas commercial heads may have up to three such modules) in order to minimize the carried mass. The head is glued to a plastic support beam which holds together the various components on the mobile side of the assembly. Actuation is provided by a cylindrical voice coil motor (VCM) located directly below the head beam, with the coil of the VCM attached to the mobile side via a stiff aluminum plate for rigid transmission, and such that the center of carried mass is coincident with the axis of the actuator. The suspension consists of two leaf springs which connect to mechanical ground and guide the head motion in the cross-track direction, suppressing all other undesirable motions of the head module relative to the tape.

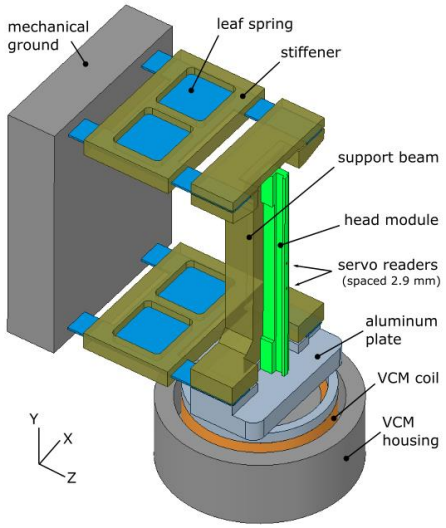

Figure 2. Schematic view of the head actuator assembly. Not shown are a flex cable connected to the head module which carries signals from the data and servo readers, and a dashpot damping unit located within the VCM, which limits the Q factor of the fundamental resonance.

This arrangement produces a plant close to that of a second-order system, i.e. a spring-mass-damper, although deviations from the ideal dynamics inevitably appear at higher frequencies (above 2 kHz), typically in connection with membrane-like eigenmodes of the leaf springs. As these undesired resonances can limit the bandwidth of the closed-loop servo system, we have optimized the layout and thickness of the springs in order to reach a suitable

compromise of membrane eigenfrequencies as high as possible, for better closed-loop bandwidth, and small enough DC stiffness, for sufficient actuation stroke to follow the LTM during tape transport.

The in-plane shape of the leaf springs comprises narrow hinge regions at the front and back to improve linearity and minimize retraction. Furthermore, the middle of the spring is overmolded with a hard plastic stiffener to up-shift the eigenfrequencies of the membrane modes. Fig. 3 shows the dependence of the overall suspension stiffness, k, and of the membrane eigenfrequencies on the thickness of the steel leaf springs t, calculated using finite-element (FE) modeling. As expected from stiffness theory, the dependence of k on t follows a power law with exponent of approximately 3 (fit: 2.78). Based on these plots we selected a spring thickness of 200 µm for the realization of the actuator, targeting a stiffness slightly over 8 kN/m and a first undesired resonance around 7 kHz.

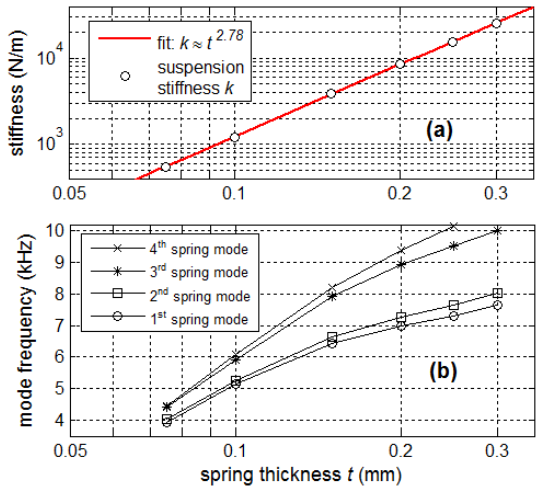

Figure 3. Calculated overall suspension stiffness (a) and leaf spring eigenmode frequencies (b), vs. thickness t of the leaf springs. The mobile mass in the FE analysis is 1.8 g, and the Young's modulus used for the spring steel was 193 GPa.

Fig. 4 shows measurements of the frequency response of the built actuator, which was also used for the experiments of this paper. The Laser Doppler Vibrometer (LDV) measurement was performed monitoring the Y position of the top face of the head module while running a frequency sweep on the VCM coil current. The second measurement was performed with tape running over the head module and using the track-following servo system to estimate the lateral position of the head while a chirp was applied on the VCM current. The two measurements agree closely, with the exceptions of a magnitude dip at ~ 380 Hz which is due to a less rigid mounting of the assembly in the tape path than on the LDV's optical bench, and of a gradual drop in phase, beyond ~ 1kHz, which is associated with delays in the closed loop servo system, as discussed in Sect V. Comparing the measured responses with the FE model forecast, we observe that the real actuator is considerably less stiff than expected, with the assembly's fundamental resonance down-shifted from ~310 Hz to ~250Hz, and the first disturbance associated with a leaf-spring mode from ~ 7kHz to ~4.5 kHz. The cause for this discrepancy is difficult to ascertain, but it is consistent with the shifts obtained when running the FE model under the assumption that shear forces are not transmitted across the interfaces between the steel leaf springs and the overmolded plastic stiffeners, i.e. that there is partial delamination at these locations.

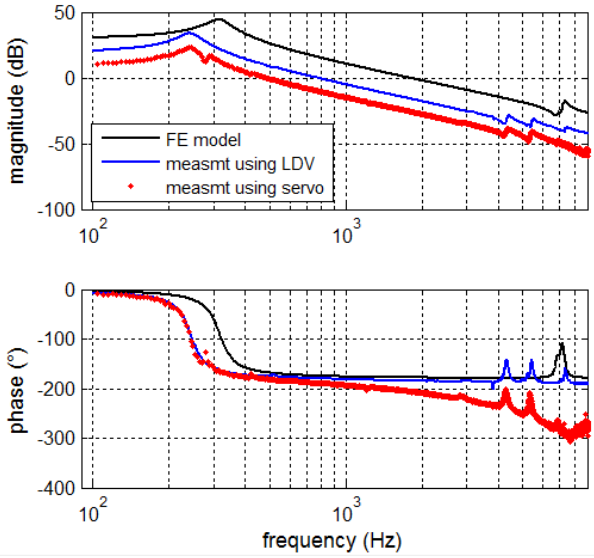

Figure 4. Frequency response of the actuator measured using an LDV (blue) and in the tape path using the track-following servo system (red), compared with a FE model (black). The magnitude plots are offset for clarity.

IV. Tape Path, LTM and Measurement Noise

The main disturbance in track-following operation is the LTM of the flexible medium [8]. To reduce the effects of the LTM in the track-following control system a high-precision tape transport system was used. The experimental tape path is depicted in Fig. 5 and has been described in more detail in [4]. It consists of four rollers that use pressured air bearings rather than ball bearings to reduce periodic disturbances that typically result from ball bearing imperfections and wear. To reduce high-frequency effects from the contact of the roller flanges with the tape edge, all four rollers are of a flangeless design. Therefore in this tape path design the tape motion is only constrained by the reel flanges which results in a rather high-amplitude LTM disturbance. However, the high amplitude motion appears only at low frequencies and is mainly due to stack shifts and periodic reel disturbances. Stack shifts are created by tape-stacking irregularities in the reel which generate high-amplitude, low-frequency motion that is repeatedly observed at the same longitudinal position. The periodic LTM is time-varying and appears at a frequency that is determined by the rotation frequency of the reel motors, typically between 10-30 Hz.

Figure 5. Photograph of the experimental tape path.

Fig. 6 shows time domain plots of typical lateral tape motion waveforms captured in open-loop at tape transport velocities of 4.08 m/s and 1.23 m/s. The peak-to-peak amplitude of the periodic effects is approx. 10-20 µm and the frequency is determined by the tape speed and the reel radii. The power spectral density of the LTM measured using the servo pattern at different tape speeds is plotted in Fig. 7 As shown in the figure, a higher tape speed results in a disturbance that has higher frequency components and thus the requirements for the closed-loop bandwidth become more demanding with increasing tape speed. Besides the disturbance characteristics, the tape speed also determines the update rate of the position estimates generated by the servo pattern and therefore the sampling rate of the synchronous closed-loop control system.

Another important consideration for achieving nanoscale track-following performance is the resolution of the position estimate. In fact, as the closed-loop bandwidth is increased, more measurement noise enters the feedback loop and introduces random positioning errors. The resolution of the position measurement can be estimated by analyzing the noise floor of the power spectral density of the LTM measured using the servo pattern. Specifically, we extrapolate the noise floor observed at high frequencies (above 5 kHz) over the full bandwidth and integrate this area to obtain an estimate of the position measurement resolution, i.e. the total noise in the position estimate. The standard deviation of the noise estimated from the experimentally measured position signals is approximately 6 nm over the whole speed range as shown in Fig. 8. At higher tape speeds, the increased sampling of the position measurement places more of the measurement noise outside the frequency range that impacts the control system. This is illustrated in Fig. 8 where the resolution of the position measurement as a function of tape speed is calculated over a 10 kHz bandwidth. With increasing tape speed the noise within this 10 kHz bandwidth decreases and hence enables an increase of the closed-loop bandwidth at higher tape speeds.

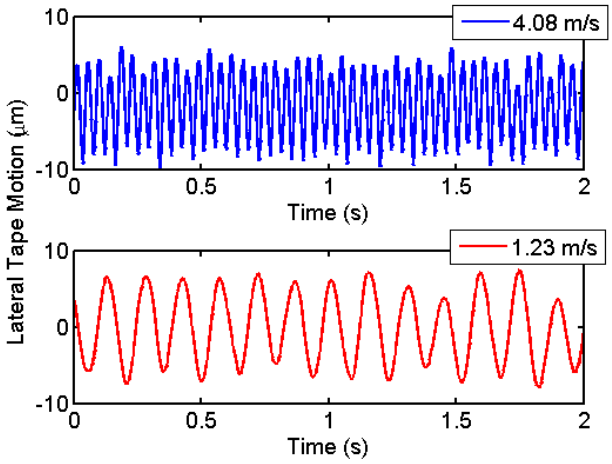

Figure 6. Time domain trace of lateral tape motion captured at 4.08 m/s and 1.23 m/s.

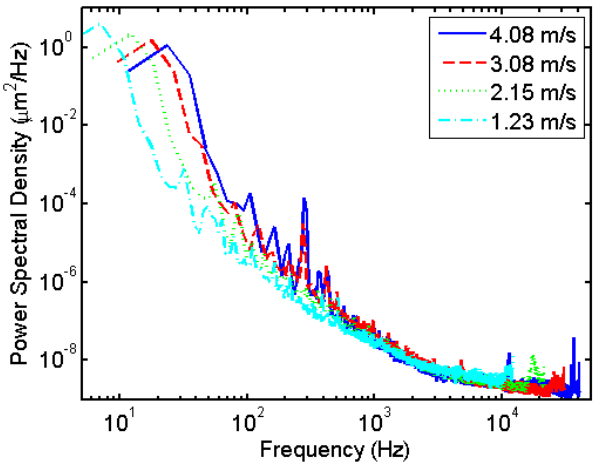

Figure 7. Power spectral density of lateral tape motion captured at various tape speeds.

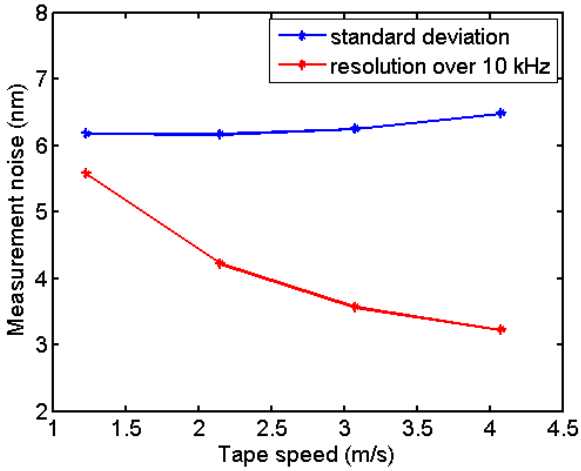

Figure 8. Resolution of position error signal measurement.

V. H_∞ TRACK-FOLLOWING CONTROL SYSTEM

A block diagram of the closed-loop track-following system is shown in Fig. 9. The controller K provides the control signal for adjusting the lateral position of the head via the head actuator to follow the position of the tape denoted by d_{LTM}. The lateral dynamics of the head actuator described in Section II are captured by the second-order transfer function G. The position error signal PES that measures the error between the position of the tape and the head is affected by the noise n and the measurement delay D. The delay is determined mainly by the servo pattern format, i.e., the subframe length d, see Fig. 1, and the tape speed v_{tape}. To characterize the speed-dependent delay in our experimental platform, a model was used to fit the phase response data captured during actuator identification at each tape speed, as shown in Fig. 10. The points correspond to the experimental phase response data for different tape speeds and the lines to a model fit created using the estimated delay parameter.

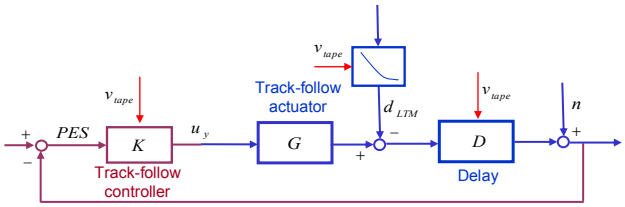

Figure 9. Schematic diagram of the track-following control system.

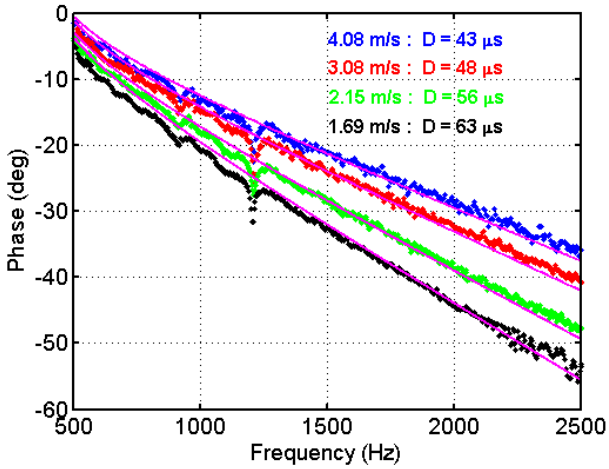

Figure 10. Estimation of measurement delay at various tape speeds.

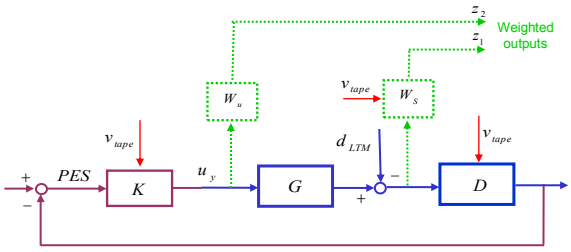

Figure 11. Block diagram of H_∞ control formulation.

The H_∞ control framework is employed to design the track-following controller K. To take into account the tape-speed-dependent characteristics of the LTM and the system delay, H_∞ controllers were optimized for each tape operating speed. This allows further optimization of the controllers compared to the control design in our previously reported demonstration [4]. The H_∞ control architecture is depicted in Fig. 11. The requirements on the closed-loop performance along with the characteristics of the LTM disturbance were specified by the so-called weighting transfer functions W_u and W_s. The speed-dependent closed-loop bandwidth requirements were captured by the transfer function W_s. Furthermore, W_s was enhanced with a second-order band-pass filter to improve disturbance rejection at the frequencies of the periodic disturbances created by the reels. The frequency of the reel periodic disturbances is also a function of the tape speed. Furthermore, to capture the time-varying nature of the disturbance due to the change in the reel radii, the width of the band-pass filter was increased. The limitations on the control effort are specified by the weighting transfer function W_u. The feedback controller K is obtained by formulating the H_∞ optimization problem using the general control configuration [9]. In this configuration, the control architecture is expressed in terms of a generalized plant P, and a generalized feedback controller K. The task of the control design is to find a controller K that minimizes the H_∞ norm of the transfer function T_{zw} between the exogenous input, $w = [d_{LTM}]$, and the exogenous outputs, $z = [z_1 \;\; z_2]^T$. In general, it is computationally simpler for the H_∞ algorithm to find a sub-optimal controller K that gives an upper bound γ to the H_∞ norm. That is, $\|T_{zw}\|_\infty < \gamma$.

Using H_∞ synthesis, a 8th order controller is obtained for each tape operating speed. Fig. 12 shows a comparison of the sensitivity closed-loop transfer functions relating the LTM disturbance with the positioning error PES for two tape speeds. The achieved closed-loop bandwidth ranges from approx. 600 Hz for low tape speeds to approx. 1 kHz for high tape speeds. The selected speed-dependent closed-loop bandwidth balances the conflicting requirements for tracking the high frequency disturbances especially at high speeds, while maintaining minimal amplification of the measurement noise especially at low speeds.

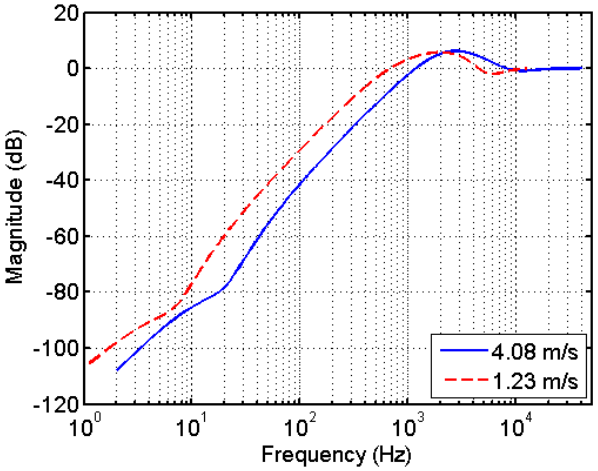

Figure 12. Magnitude response of sensitivity closed-loop transfer function at 4.08 m/s and 1.23 m/s.

VI. TRACK-FOLLOWING PERFORMANCE

Closed-loop track-following experiments were performed over a range of tape speeds using the high-bandwidth actuator described in Sect. III, the tape path described in Sect. IV and a hardware prototyping platform that was described previously in [2]. The actuator was equipped with a beveled [3] GMR tape head with 3.5-µm-wide servo readers. The hardware platform consists of an FPGA board, a current driver and a host computer as well as the electronics card from an IBM TS1140 tape drive that provides reel-to-reel control for the tape path. The drive card is also used as the front-end for the tape head, providing bias currents to the GMR elements as well as amplification, filtering and analog-to-digital conversion of the signals from the GMR readers. Samples of the servo readback waveform obtained by the electronics card are fed to the FPGA board, in which the servo channel described in Sect. II was implemented. The track-following controller described in Sect. V runs on a Nios® II soft-core microprocessor that was also implemented in the FPGA. The track-following controller is run synchronously in an interrupt-driven mode, with an interrupt provided by the servo channel whenever a new head position estimate is available. In the synchronous mode of operation the sampling frequency of the track-following system depends on the tape speed and ranges from 24.6 kHz to 81.6 kHz for speeds from 1.23 m/s to 4.08 m/s. A digital-to-analog converter (D/A) on the FPGA board is used to feed the controller output to a current amplifier that drives the head actuator.

The closed-loop track-following experiments were performed over the full speed range of an IBM TS1140 enterprise class tape drive. Fig. 13 presents time-domain plots of the closed-loop PES measured at the highest and lowest tape speeds investigated, namely, 1.23 m/s and 4.08 m/s. The PES measured at 1.23 m/s exhibits a standard deviation σ-PES of 9.5 nm compared to 10.1 nm measured at 4.08 m/s. Although the difference in the frequency content of the LTM disturbances and the distribution of noise in the position estimates is the largest at these two tapes speeds, the difference in closed-loop track-following performance is only 0.6 nm. As described above, this was achieved by balancing the conflicting requirements of tracking the high-frequency disturbances, in particular at high speeds, while maintaining minimal amplification of the measurement noise at the low speeds, where increased delay effects are observed. The result of these trade-offs can partially be seen in the power spectral density plots of the two PES data sets shown in Fig. 14. In the plot it can be seen that the lower bandwidth of the 1.23 m/s controller results in more spectral content in the range of 300 Hz to 1 kHz. A higher bandwidth controller would result in stronger suppression of disturbances in this frequency range, but more amplification of the position estimation noise at higher frequencies (in the range of 1-5 kHz), and hence a larger σ-PES.

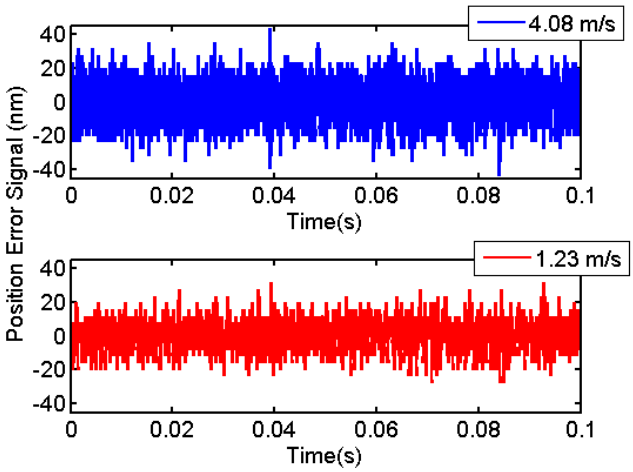

Figure 13. Time-domain closed-loop PES at 4.08 m/s and 1.23 m/s.

The standard deviation of the PES as a function of tape velocity is plotted for seven representative tape speeds in the upper panel of Fig. 15. The standard deviation of the PES ranges from 9.0 to 10.1 nm over the speed range of 1.23 to 4.08 m/s with an average value of 9.4 nm, demonstrating the effectiveness of our design methodology in achieving uniform track-following performance over the speed range.

Previously, relatively large differences in track-following performance have been reported as a function of track-following reference position on timing-based servo patterns [4]. Such differences could arise from the difference in pattern delay, which varies as a function of the lateral position relative to the servo pattern centerline, or also due to variations in the quality of the servo pattern across the width of the pattern. The lower panel of Fig. 15 presents the σ-PES measured versus reference position across the width of the servo pattern at a tape speed of 2.61 m/s. The consistent performance observed here is an indication of a

high quality of servo formatting and that the position dependent delay effects of approximately +/- 2 μs for the servo pattern used here are not significant.

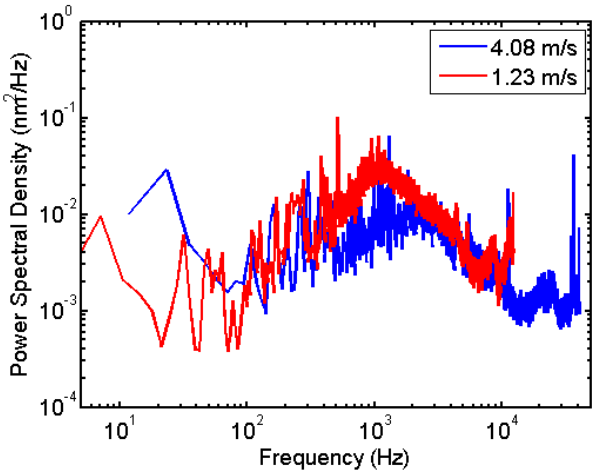

Figure 14. Power spectral density of closed-loop PES at 4.08 m/s and 1.23 m/s.

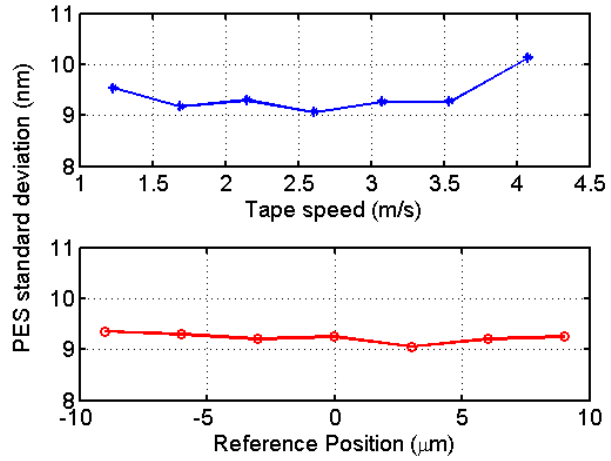

Figure 15. PES standard deviation as a function of tape speed and reference position.

VII. Conclusion

In this paper, we have demonstrated the potential to achieve nanometer-scale track-following position control in a reel-to-reel magnetic tape system. Specifically, we demonstrated a record closed-loop performance characterized by a standard deviation in PES between 9.0 and 10.1 nm over a tape speed range of 1.23 to 4.08 m/s, with an average standard deviation of 9.4 nm over this speed range. This is roughly a 40% reduction in positioning error compared to our previously reported record [4]. This result was achieved through the combination of advances in several elements of the track-following system, including an optimized servo channel, an experimental timing-based servo pattern, a prototype high-bandwidth head actuator, an experimental flangeless tape transport system, a delay-optimized hardware prototyping platform and a set of track-following controllers optimized for each tape speed using the H_∞ control framework. This work demonstrates the potential for continued aggressive track-density scaling that will be required to enable future tape cartridge capacities of 100 TB and beyond [1].

* Linear Tape Open and LTO are trademarks of HP, IBM and Quantum in the US and other countries.

Acknowledgment

The authors are grateful to FujiFilm for supplying the prototype media sample and to Evangelos Eleftheriou for his support of this work.

References

[1] International Storage Industry Consortium (INSIC) 2012-2022 Tape Roadmap, http://www.insic.org/news/2012Roadmap/12index.html.

[2] S. Furrer et al., "85.9 Gb/in^2 recording areal density on barium ferrite tape," accepted for publication in *IEEE Trans. Magn.,* Sep. 2014.

[3] G. Cherubini et al., "29.5 Gb/in^2 recording areal density on barium ferrite tape," *IEEE Trans. Magn.,* vol. 47, no. 1, pp. 137-147, Jan. 2011.

[4] M. A. Lantz, G. Cherubini, A. Pantazi and J. Jelitto, "Servo-pattern design and track-following control for nanometer head positioning on flexible tape media", *IEEE Trans. Control Syst. Technol*., vol. 20, no. 2, pp. 369-381, Mar. 2012.

[5] R. C. Barrett, E. H. Klaassen, T. R. Albrecht, G. A. Jaquette, and J. H. Eaton, "Timing-based track-following servo for linear tape systems," *IEEE Trans. Magn*., vol. 34, pp. 1872–1877, Jul. 1998.

[6] S. Furrer, P.-O. Jubert, G. Cherubini, R. D. Cideciyan, and M. A. Lantz, "Analytical expressions for the readback signal of timing-based servo schemes," *IEEE Trans. Magn.*, vol. 48, no.11, pp. 4578-4581, Nov. 2012.

[7] G. Cherubini, E. Eleftheriou, J. Jelitto, and R. Hutchins, "Synchronous servo channel design for tape drive systems," in *Proc. 17th Ann. ASME Information Storage and Processing Systems Conf*., Santa Clara, CA, 2007, pp. 160–162.

[8] A. Pantazi, J. Jelitto, N. Bui, and E. Eleftheriou, "Track-following in tape storage: Lateral tape motion and control," *Mechatronics*, vol. 22, no. 3, pp. 361-367, 2012.

[9] S. Skogestad and I. Postletwaithe, *Multivariable Feedback Control*. New York: Wiley, 1996.